Experimental Assessment of Energy Requirements and Tool Tip Visibility for Photoacoustic-Guided Endonasal Surgery

Muyinatu A. Lediju Bell,[*a] Alicia B. Dagle,[a,b] Peter Kazanzides,[a] and Emad M. Boctor[a,c]

[a]Johns Hopkins University, Department of Computer Science, Baltimore, MD, USA
[b]Clark University, Department of Physics, Worcester, MA, USA
[c]Johns Hopkins University, Department of Radiology, Baltimore, MD, USA

ABSTRACT

Endonasal transsphenoidal surgery is an effective approach for pituitary adenoma resection, yet it poses the serious risk of internal carotid artery injury. We propose to visualize these carotid arteries, which are hidden by bone, with an optical fiber attached to a surgical tool and a transcranial ultrasound probe placed on the patient's temple (i.e. intraoperative photoacoustic imaging). To investigate energy requirements for vessel visualization, experiments were conducted with a phantom containing *ex vivo* sheep brain, *ex vivo* bovine blood, and 0.5-2.5 mm thick human cadaveric skull specimens. Photoacoustic images were acquired with 1.2-9.3 mJ laser energy, and the resulting vessel contrast was measured at each energy level. The distal vessel boundary was difficult to distinguish at the chosen contrast threshold for visibility (4.5 dB), which was used to determine the minimum energies for vessel visualization. The blood vessel was successfully visualized in the presence of the 0-2.0 mm thick sphenoid and temporal bones with up to 19.2 dB contrast. The minimum energy required ranged from 1.2-5.0 mJ, 4.2-5.9 mJ, and 4.6-5.2 mJ for the 1.0 temporal and 0-1.5 mm sphenoid bones, 1.5 mm temporal and 0-0.5 mm sphenoid bones, and 2.0 mm temporal and 0-0.5 mm sphenoid bones, respectively, which corresponds to a fluence range of 4-21 mJ/cm^2. These results hold promise for vessel visualization within safety limits. In a separate experiment, a mock tool tip was placed, providing satisfactory preliminary evidence that surgical tool tips can be visualized simultaneously with blood vessels.

Keywords: transcranial photoacoustic imaging, laser safety, surgical tool visualization, maximum permissible exposure (MPE), energy limits, phased array ultrasound probe, endonasal transsphenoidal surgery, head phantom

1. INTRODUCTION

Endonasal transphenoidal surgery is the most common approach to remove pituitary adenomas [1]. This minimally-invasive resection is performed by inserting surgical instruments through the nostril, nasal septum, and sphenoid sinus. The surgeon then drills through the sphenoid bone and uses a curette to remove the tumor. An endoscope accompanies these surgical tools, providing a visual of the superficial structures, but neglecting to locate the internal carotid arteries which may lie in the drilling path. Although MRI and CT scans provide helpful preoperative images, there is currently no real-time imaging modality to effectively warn the surgeons approaching these blood vessels.

To overcome this limitation, we propose photoacoustic imaging with a transducer placed on the patient's temple and an optical fiber, coupled to a laser on one end with the opposite end attached to a surgical tool (e.g., a drill). The surgical tool and fiber would be inserted through the nasal passage, where it would illuminate the tool tip and drilling area, specifically the sphenoid bone which has a thickness of 0.4-8.8 mm [2, 3]. We envision the laser causing the surgical tool tip and underlying blood vessels to generate photoacoustic signals that can be visualized in intraoperative photoacoustic images [4].

When implementing this procedure, it is vital to consider limitations such as the acceptable laser exposure for brain tissue and other surrounding components. If the energy exposure is too high, the tissue may coagulate or even vaporize. Laser radiation causes thermal effects depending on the wavelength, power, energy, beam

*E-mail: muyinatu.ledijubell@jhu.edu

Photons Plus Ultrasound: Imaging and Sensing 2016, edited by Alexander A. Oraevsky, Lihong V. Wang
Proc. of SPIE Vol. 9708, 97080D · © 2016 SPIE · CCC code: 1605-7422/16/$18 · doi: 10.1117/12.2213220

diameter, and absorption spectrum of the tissue. Other factors include the volume of circulating blood, specific heat, thermal conductivity, non-homogeneity, and optical properties such as transmission, reflection, absorption, and scattering [5]. Although bone and brain have significantly different optical properties from skin, we will assume that the limits for skin apply to this study, which is a rather conservative assumption.

The goals of this paper are to quantify the minimum contrast for visibility of blood vessels, specify the minimum energy at which this contrast is achieved, and compare these energy measurements to the ANSI laser safety limits [5]. In doing so, we aim to determine whether real-time photoacoustic imaging may be employed to safely visualize blood vessels intraoperatively during endonasal transsphenoidal surgery. We also provide preliminary evidence of how this information may be used in conjunction with visualization of surgical tool tips.

2. METHODS

2.1 Equipment and Materials

An Nd:YAG laser with an optical parametric oscillator coupled to a 6 mm diameter optical fiber cable was operated with a pulse duration of 5 ns, and a pulse frequency of 10 Hz. The wavelength was 760 nm for the duration of the experiments, which corresponds with the peak in the optical absorption spectrum of deoxygenated hemoglobin [6]. The ANSI laser safety limit at this wavelength is 26.4 mJ/cm^2 [5]. A SonixTouch Ultrasound Scanner was used in conjunction with an ATL P4-2 transcranial ultrasound probe (2-4 MHz bandwidth). Laser energy was measured using an energy meter and averaged over 5 recorded energies to determine the mean energy applied during the experiments.

2.2 Phantom Setup

The phantom setup consisted of a small container resting inside a larger container to depict the anatomical structure of the human head, as shown in Figs. 1(a)-(c). The side of the outer container was cut and replaced by an acoustic window. The bottom of the inner container was cut and replaced with Saran wrap, which acted as an optical window for the laser beam. A vessel, used to mimic the internal carotid artery, was attached to the bottom of the inner container, approximately 1 mm away from the Saran wrap. This vessel consisted of Ultra-Clear Tygon PVC tubing (inner diameter: 4.8 mm, outer diameter 6.4 mm) and was filled with *ex vivo* bovine blood mixed with 3.8% sodium citrate tribasic as an anticoagulant, which mimics known physiological levels [7, 8]. The diameter of the tube is consistent with that of the internal carrotid arteries, which can range from 3.7-8 mm for patients age 12 or older [9].

The bottom of the outer container was lined with plastisol with a cut-out for the *ex vivo* sheep brain, which was inserted to mimic the optical and acoustic properties of human brain. The brain was wrapped in Saran wrap to keep it intact. A small piece of brain tissue (removed from the brainstem and cerebellum), was inserted between the blood vessel and the bottom of the inner container, resulting in the blood vessel being located approximately 1 mm away from the inner container. This inner container was then added to the phantom setup, which resulted in the blood vessel being completely surrounded by brain tissue as shown in Figs. 1(b)-(c). Water filled the remainder of the outer container.

Human cadaver skull bone specimens of thickness 0.5-2.5 mm (pictured in Fig. 1(d) and described in our previous publication [10]) were utilized to mimic the sphenoid and temporal bones. One cadaveric skull specimen was placed between the laser and brain tissue to mimic the sphenoid bone. The laser was placed approximately 1 mm from the sphenoid bone, and 2-3 mm from the blood vessel. Another cadaveric skull specimen was placed between the ultrasound probe and brain tissue to mimic the temporal bone. The placement of these two bone specimens is shown in Figs. 1(b)-(c), and the specific specimen utilized was varied to achieve all possible combinations of temporal and sphenoid bone thicknesses.

Photoacoustic data were acquired with the laser consistently placed above the center of the vessel where the photoacoustic signals from the proximal and distal boundaries were strongest [4]. Note that the terms proximal and distal are defined relative to the ultrasound probe. For each combination of temporal and sphenoid bone thicknesses, the laser energy was decreased from 9.3 mJ until the vessel boundaries were not visible in

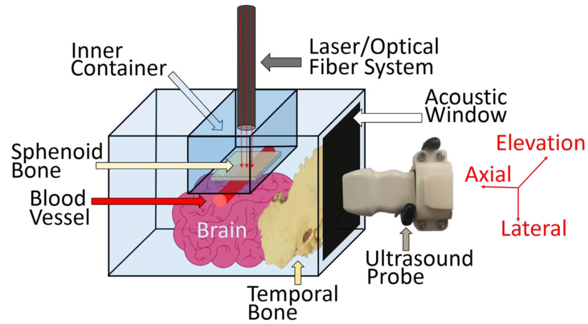

(a)

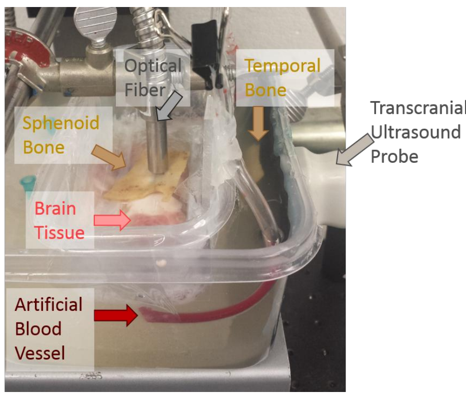

(b)

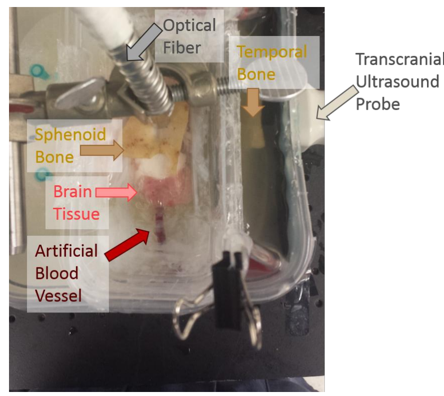

(c)

(d)

Figure 1. (a) Schematic diagram of phantom used for testing. Photographs of the phantom setup with blood vessel surrounded by brain tissue from two different perspectives: (b) oblique view and (c) aerial view. (d) Cadaveric skull specimens used in place of the sphenoid and temporal bone in phantom construction.

real-time images of the raw channel data. Ten raw RF photoacoustic data were averaged to display one delay-and-sum beamformed image. Ultrasound images were additionally acquired with each variation of temporal bone thickness.

Photoacoustic image contrast was measured as follows:

$$\mathrm{C} = 20\log_{10}\frac{\mu_\mathrm{i}}{\mu_\mathrm{o}} \tag{1}$$

where μ_i and μ_o represent the image data with regions of interest located inside and outside the distal blood vessel boundary.

2.3 Addition of Tool Tip

The phantom was modified to include a metal component which mimics the surgical drill tip. Loctite super glue was utilized to adhere a 2.38 mm diameter metallic ball (similar to the drill size) to the end of a paper clip. The paper clip was bent into a desired position and affixed to the outside of the inner container. This artificial tool tip was placed approximately 2 mm from the vessel in the probe's axial dimension. The laser energy was

Figure 2. Experimental setup showing the tool tip placed above the sphenoid bone and to the left of the blood vessel (i.e. distal to the vessel relative to the ultrasound probe, which is not shown, but is located to the right of the image).

9.3 mJ and the laser position was centered above either the tool tip, the distal vessel boundary, the center of the vessel, or the proximal vessel boundary. Photoacoustic data were acquired with no bone in place, with the 1.0 mm thick sphenoid bone placed between the tool tip and vessel, as shown in Fig. 2 (note that the sphenoid bone is submerged in water in this case, unlike the previous setup), then with the 1.5 mm thick temporal bone added to this setup.

3. RESULTS

3.1 Minimum Energy and Fluence Requirements

Example ultrasound and photoacoustic images acquired with the maximum laser energy (9.3 mJ) are shown in Fig. 3. In the ultrasound images, it was difficult to distinguish features located behind the bone when the temporal bone thickness was greater than 1.5 mm, although the vessel was still fairly visible in the photoacoustic images (see Fig. 3(c)). In the photoacoustic images, vessel boundaries were successfully visualized in the presence of the 0.5-2.0 mm thick sphenoid and temporal bones with up to 19.2 dB contrast.

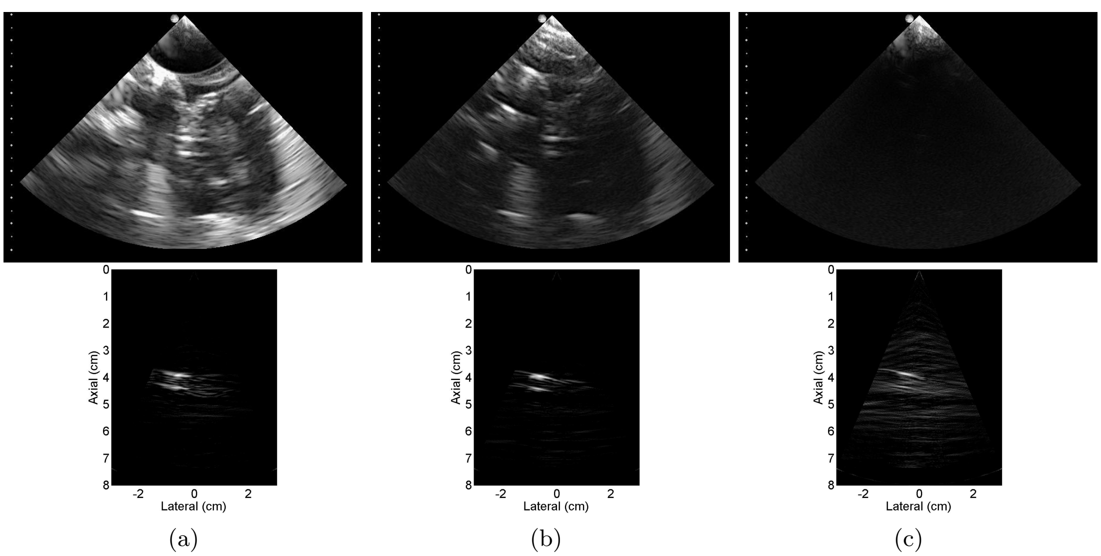

Figure 3. Ultrasound (top) and photoacoustic (bottom) images of the vessel filled with blood, surrounded by brain and water with the temporal bone thickness varied as follows: (a) 0 mm (no bone), (b) 1.0 mm bone, and (c) 2.0 mm bone. No sphenoid bone was present to obtain these images. The photoacoustic images are displayed with 20 dB dynamic range.

The threshold contrast for vessel visibility was empirically determined to be 4.5 dB, and it was used to assess the minimum energy required to visualize blood in the presence of bone. Generally, the distal boundary was

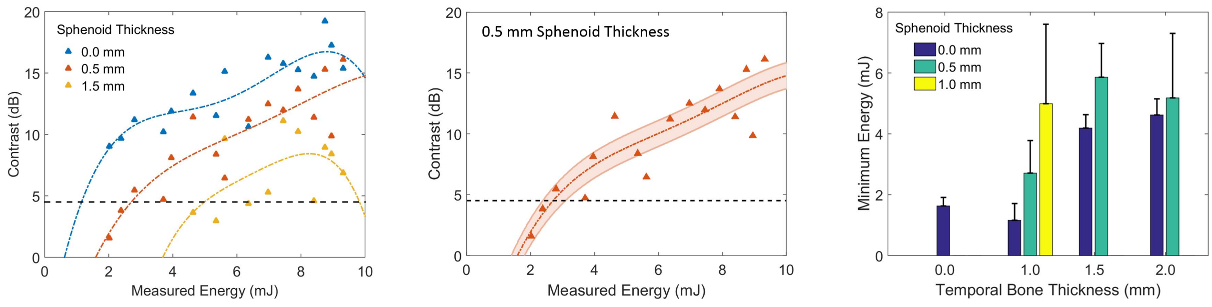

Figure 4. (a) The 1.0 mm thick temporal bone was held constant as sphenoid bone thickness was varied. Best fit lines were drawn for each data set and extrapolated. (b) The intersection of the line with the threshold contrast was found to be minimum energy for visibility, energy error corresponds to horizontal error in shaded region. (c) Minimum energy is plotted as a function of both sphenoid and temporal bone thickness. Error bars are derived from energy error as portrayed with the shaded error bars.

poorly visualized at this threshold value, although for the same energy, the proximal boundary was still visible, as evident in Fig. 3(c). A best-fit curve was extrapolated for each data set representing contrast as a function of energy for each combination of temporal and sphenoid bone thickness. Intersection with the minimum contrast for visibility (4.5 dB) was obtained if the best fit line sloped downward as energy decreased. This energy intercept was determined to be the minimum energy required for visibility. For example, Fig. 4(a) shows this intercept for the 1 mm temporal and 0-1.5 mm sphenoid bone thicknesses. The error of each fit was used to plot shaded error bars (e.g., Fig. 4(b)) and determine the error of the minimum required energy values reported in Fig. 4(c).

As shown in Fig. 4(c), the minimum energy required to visualize blood in the presence of the 1.0 mm temporal and 0-1.5 mm sphenoid bones ranged 1.2-5.0 mJ, the energy required for the 1.5 mm temporal and 0-0.5 mm sphenoid bones ranged 4.5-5.9 mJ, and the energy required for the 2.0 mm temporal and 0-0.5 mm sphenoid bones ranged 4.6-5.2 mJ. This indicates a general increase in energy required with increased bone thickness (as expected), and the corresponding fluence ranges 4-21 mJ/cm^2 for the 6 mm diameter fiber bundle utilized in these experiments. These values are within the 26.4 mJ/cm^2 safety limits for the 760 nm laser wavelength and 5 ns pulse duration [5].

3.2 Tool Tip Visualization

When the tool tip and blood were surrounded by water (with no bone present), the proximal and distal boundaries were present in addition to the tool tip, as demonstrated in Fig. 5(a). This image was created by combining multiple images obtained when the optical fiber was centered above each structure in the image, using

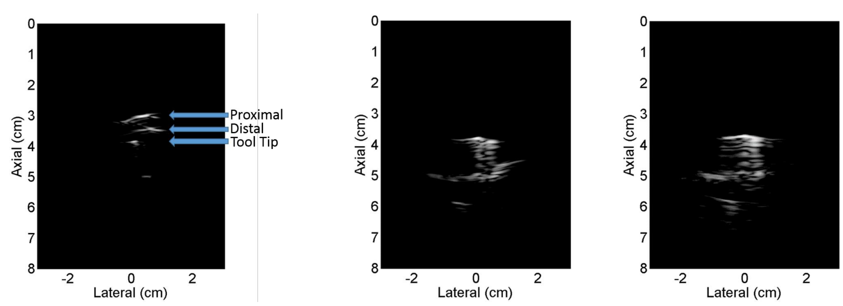

Figure 5. (a) The proximal and distal vessel boundaries and the tool tip are clearly distinguishable in the photoacoustic image created by centering the optical fiber above each structure and compounding the resulting images. Photoacoustic images were then acquired when the laser was centered above the tool tip with (b) the 1.0 mm sphenoid and (c) the 1.0 mm sphenoid and 1.5 mm temporal bones in place. Images are displayed with 15 dB dynamic range.

the same method reported in a previous publication for data obtained with the direction of the light source varied as the ultrasound probe was stationary [11]. Bone was added to the experimental setup to obtain the images shown in Figs. 5(b) and (c). When the laser was centered above the tool tip with the 1.0 mm sphenoid bone in place (Fig. 5(b)) and when the 1.5 mm temporal bone was added to this setup (Fig. 5(c)), the tool tip was visible in the same location as in Fig. 5(a) (e.g., the lateral position is approximately 0 cm), although there were additional signals that we attribute to the presence of the sphenoid bone. These signals are either photoacoustic signals generated by the fully submerged sphenoid bone (which is located between the vessel and tool tip), acoustic reflections caused by the presence of sphenoid bone and the highly reflective metal (i.e., clutter noise), or a combination of these two effects.

4. DISCUSSION

The results herein provide evidence to support multiple hypotheses presented in our previous publications, including the visualization of blood located behind bone for surgical guidance [4, 10, 12], the visualization of the tool tip and vessel in a single image [4], and the utility of contrast measurements as the sphenoid bone is removed (i.e., as sphenoid bone thickness decreases) during surgery [10]. In particular, Fig. 4 indicates that contrast generally decreases as energy decreases, and this trend can be fit to a mathematical model (i.e., the equations describing the best-fit curves). Contrast also decreased as bone thickness increased (with some exceptions likely caused by variations in laser energy, bone consistency, and vessel composition within the bone). Thus, similar mathematical models for each patient case may be extrapolated to estimate bone thickness while drilling, as suggested in our previous publication [10].

One option for implementation of the proposed approach consists of an optical fiber attached to the surgical tool to illuminate both the metal tool tip and the underlying artery. Our preliminary results shown in Fig. 5 indicate that the tool tip will potentially generate a sufficient photoacoustic signal to track the relative location between the surgical tool tip and the blood vessel boundaries, particularly after all bone has been removed and soft tissue separates the tool from the vessel. More experiments and signal processing are required to determine the source of the additional photoacoustic signals that appear when the sphenoid bone is submerged in an acoustic propagation medium (i.e., water). It is likely that these signals are a photoacoustic response from bone, given their location and our previous success with visualizing bone [4], and in this case, it is sufficient for the signal from the bone to serve as a surrogate for the location of the fiber and tool tip. However, if these signals are instead caused by acoustic reflections, they can likely be mitigated to clearly identify the signal from the tool tip by either reducing the laser energy, applying advanced reconstruction methods, and/or combining multiple images of different structures obtained by varying the direction of the light source while the ultrasound probe is kept stationary [11].

The proposed technology promises to assist the surgeon throughout the pituitary removal process by indicating relative proximity to the internal carotid arteries, thereby enabling the surgeon to avoid them before injury occurs. This is particularly helpful when the soft tissue shifts during surgery, and the preoperative images consequently become less reliable. While endoscopic images are currently available to navigate superficial structures, this technology has the added benefit of helping surgeons to visualize hidden blood vessels located in the drilling path. The inclusion of a robot has additional potential to improve navigation during this surgical procedure [13].

5. CONCLUSION

For the first time, *ex vivo* bovine blood was successfully visualized in the presence of *ex vivo* sheep brain tissue, with both anatomical structures hidden by human cadaveric skull specimens. We determined that the contrast threshold for visibility was approximately 4.5 dB. Below this value, the distal boundary was difficult to distinguish in delay-and-sum photoacoustic images. Therefore, the minimum energy required to visualize blood hidden by sphenoid and temporal bones of thickness 0.5-2.0 mm ranged 1.2-5.9 mJ, corresponding to a fluence of 4-21 mJ/cm^2, which is less than 90% of the ANSI safety limit for skin. Vessel contrast increased as sphenoid bone thickness decreased with temporal bone thickness held constant, which is representative of what the surgeon might expect to see while drilling through the sphenoid bone. Results hold promise for an intraoperative photoacoustic imaging technique to safely guide surgeons around the internal carotid arteries by providing real-time updates about the location of the surgical drill tip relative to these arteries.

ACKNOWLEDGMENTS

This work was completed as part of the NSF CSMR REU program at The Johns Hopkins University and was sponsored by NSF grant EEC-1460674 and NIH grant K99-EB018994 (awarded to M. A. Lediju Bell).

References

[1] D. Mukherjee, H. A. Zaidi, T. Kosztowski, K. L. Chaichana, R. Salvatori, D. C. Chang, and A. Quiñones-Hinojosa. Predictors of access to pituitary tumor resection in the United States, 1988–2005. *European Journal of Endocrinology*, 161(2):259–265, 2009.

[2] N. Lazaridis, K. Natsis, J. Koebke, and C. Themelis. Nasal, sellar, and sphenoid sinus measurements in relation to pituitary surgery. *Clinical Anatomy*, 23(6):629–636, 2010.

[3] W. Hosemann, R. Gross, U. Göde, T. Kühnel, and G. Röckelein. The anterior sphenoid wall: relative anatomy for sphenoidotomy. *American Journal of Rhinology*, 9(3):137–144, 1995.

[4] M. A. Lediju Bell, A. K. Ostrowski, K. Li, P. Kazanzides, and E. M. Boctor. Localization of transcranial targets for photoacoustic-guided endonasal surgeries. *Photoacoustics*, 3(2):78–87, 2015.

[5] Laser Institute of America. American national standards for safe use of lasers in health care. *ANSI Z136.3-2011*, pages 45–46, 2012.

[6] S. Prahl. Tabulated molar extinction coefficient for hemoglobin in water. Oregon Medical Laser Center, 1998. Accessed: 2015-08-01.

[7] D. M. Adcock, D. C. Kressin, and R. A. Marlar. Effect of 3.2% vs 3.8% sodium citrate concentration on routine coagulation testing. *American Journal of Clinical Pathology*, 107(1):105–110, 1997.

[8] G. Brecher and E. P. Cronkite. Morphology and enumeration of human blood platelets. *Journal of Applied Physiology*, 3(6):365–377, 1950.

[9] H. Takegoshi and S. Kikuchi. An anatomic study of the horizontal petrous internal carotid artery: Sex and age differences. *Auris Nasus Larynx*, 34(3):297–301, 2007.

[10] M. A. Lediju Bell, A. K. Ostrowski, K. Li, P. Kazanzides, and E. Boctor. Quantifying bone thickness, light transmission, and contrast interrelationships in transcranial photoacoustic imaging. In *SPIE BiOS*, pages 93230C–93230C. International Society for Optics and Photonics, 2015.

[11] M. A. Lediju Bell, X. Guo, D. Y. Song, and E. M. Boctor. Transurethral light delivery for prostate photoacoustic imaging. *Journal of Biomedical Optics*, 20(3):036002–036002, 2015.

[12] M. A. Lediju Bell, A. K. Ostrowski, P. Kazanzides, and E. Boctor. Feasibility of transcranial photoacoustic imaging for interventional guidance of endonasal surgeries. In *SPIE BiOS*, pages 894307–894307. International Society for Optics and Photonics, 2014.

[13] S. Kim, H. J. Kang, A. Cheng, M. A. Lediju Bell, E. Boctor, and P. Kazanzides. Photoacoustic image guidance for robot-assisted skull base surgery. In *Robotics and Automation (ICRA), 2015 IEEE International Conference on*, pages 592–597. IEEE, 2015.